Available online at www.sciencedirect.com
ScienceDirect
Ceramics International 37 (2011) 313–319
CERAMICS INTERNATIONAL
www.elsevier.com/locate/ceramint

Fabrication of aluminum nitride coatings by electrophoretic deposition: Effect of particle size on deposition and drying behavior

H. Abdoli [a], M. Zarabian [b], P. Alizadeh [a,*], S.K. Sadrnezhaad [b]

[a] Department of Materials Science and Engineering, Tarbiat Modares University, P.O. Box 14115-143, Tehran, Iran
[b] Department of Materials Science and Engineering, Sharif University of Technology, P.O. Box 11365-9466, Azadi Avenue, Tehran 14588, Iran

Received 28 January 2010; received in revised form 12 May 2010; accepted 28 August 2010
Available online 25 September 2010

Abstract

Electrophoretic technique was used to deposit micro- and nano-sized aluminum nitride coatings on stainless steel surfaces by using a well-dispersed stable suspension produced by addition of AlN powder plus a small amount of iodine to ethanol. Parabolic regime governed the deposition. Electrophoretic deposition for 240 s at 100 V resulted in formation of a uniformly dense film on the top, but a porous inhomogeneous layer at the bottom. This was attributed to fast deposition of coarse particles and/or agglomerates at large electric fields. After drying, micro-sized particles led to a uniform crack-free interface while nano-particles resulted in fragmented non-cohesive layers. Weight loss measurements revealed higher drying rates for micro-layer as compared to nano-cover. This seemed owing to the larger pore sizes and lower specific surfaces of the former. Stress inducement by lateral drying of small capillaries led to crack initiation from the edges and its propagation across the surfaces. This resulted in fragmentation of the samples due to their delamination. Effect of deposition rate on particles packability was also investigated.

Keywords: A. Drying; Electrophoretic deposition; Microstructure; Kinetics

1. Introduction

Electrophoretic deposition (EPD) is a rapid developing technology capable of producing ceramic coatings [1,2], functionally graded materials [3,4], thin and thick layers [5,6], porous materials [7] and nanoparticle deposits [8]. Various materials including alumina [9,10], zirconia [11,12], hydroxyapatite [13] and carbon nanotube [14] have previously been deposited by this technique. EPD has received increasing attention because of simplicity, low cost, applicability to different materials, possibility of using complicated substrates and capability of scale-up to large production rates [15,16].

EPD comprises two steps [15]: (i) charged colloidal suspended particles are forced to migrate towards an electrode under the applied electric field and (ii) the particles depositing on the working electrode form a coherent dense layer. These processes follow drying and densification by sintering or curing. Although many efforts have been devoted to understand this process, there are still many parameters that must be worked on to control the formation of the EPD layers.

Two types of parameters are to be considered to control the morphology and microstructure of the electrophoretically deposited layer [17–19]: (i) physical factors comprising of the applied voltage, deposition time, suspension concentration and substrate specifications and (ii) chemical parameters including zeta potential, liquid-phase dielectric constant, raw-materials morphology and their particle size plus conductivity, viscosity and stability of the suspension. Kinetic equations have previously been developed to predict the effect of the influential parameters on the rate of deposition [20,21].

Packing behavior of the colloidal particles is influenced by particle size, particle concentration, interaction between particles and rheological properties of the mixture. Packing compactness affects shrinkage, density and microstructure of the consolidated ceramic objects [22]. A uniform green density has substantial effect on controlling the sintering contraction and microstructural flaws which may cause in-use component fail [23]. It is commonly accepted that ceramic compacts having high green density and small uniform pores can most effectively be densified by sintering [24,25].

* Corresponding author. Tel.: +98 21 8288 4399; fax: +98 21 8288 3381.
E-mail addresses: habdoli@alum.sharif.edu (H. Abdoli), p-alizadeh@modares.ac.ir (P. Alizadeh).

0272-8842/$36.00 © 2010 Published by Elsevier Ltd and Techna Group S.r.l.
doi:10.1016/j.ceramint.2010.09.012

As a colloidal process, EPD is associated with a major obstacle after applying the deposition. Drying often causes problems because of removal of liquid vehicle necessary for processes which can lead to problems associated with dimensional control, segregation, and cracking [25]. Several approaches have been suggested by Sarkar et al. [26] to avoid cracking during drying.

Only few publications are available on the effect of particle size and particle size distribution on deposition [27,28], suspension stability [29], electrophoretic mobility [30], particle packing behavior [24] and crack formation during the drying stage of the EPD process. To the best knowledge of the authors, there is no publication accessible on behavior of different sized powders during EPD and drying. This work aims to investigate the effect of particle size on packing, drying, morphology and microstructure of the EPD AlN coating.

2. Materials and methods

Micro-sized aluminum nitride designated as m-AlN supplied by Aldrich Co., USA and nano-sized aluminum nitride powder designated as n-AlN supplied by Plasma Chem. GmbH, Germany were used as raw materials in this research. Morphology of both powders is shown in Fig. 1. It denotes that both powders have a range of shapes. XRD analysis confirmed that both powders crystal symmetry was mostly hexagonal (wurtzite phase), therefore, the surface chemical behavior of both powders was nearly identical. The other characteristics of the samples are listed in Table 1. Particle size distribution of m-AlN powder analyzed by Fritsch particle size 'analysette 22' is shown in Fig. 2.

Table 1
The characteristics of micro-sized and nano-sized AlN powders.

Specimen	Purity (%)	Particle size range	Mean particle size	Surface area (m^2/g)
m-AlN	≥98	<10 μm	2.9 μm	2.74
n-AlN	≥95	<200 nm	50 nm	18

Three organic substances used in this investigation were: (i) methanol (>99.9% Merck, Germany); (ii) 2-propanol (99.96%, Merck, Germany) and (iii) absolute ethanol (99.99%, Merck, Germany). Non-aqueous suspension was prepared by adding 0.2 g of AlN powder to 20 ml of the organic substance. Since the most uniform coating was obtained from the ethanol-based suspension, further experiments were conducted with this mixture. Addition of iodine (with concentration of 0.02 g/l) to ethanol generates hydrogen iodine (HI) via the following reaction [31,32]:

$$CH_3-CH_2-OH(\text{Ethanol}) + I_2 \leftrightarrow ICH_2-CH_2-OH + HI \quad (1)$$

A proton is quickly produced by dissociation of HI and particles are charged via protons adsorption:

$$HI \rightarrow H^+ + I^- \quad (2)$$

In order to achieve a well-dispersed homogenous suspension considered crucial in EPD procedure, the mixture was ultrasonicated for 60 min. Zeta potential of suspensions were evaluated by Malvern Zetasizer-3000. To achieve deposition, an electrophoretic cell was designed with certain inter-electrode spacing of 10 mm. Both electrodes were made of stainless steel sheets having ~300 μm thickness. Prior to deposition, the metallic substrates were washed with detergent and degreased with acetone and then dried in the air at the room temperature. One side of the cathode was masked with a non-conducting tape and the other side was coated. The surface area of the cathode was 1 cm^2.

A constant voltage of 100 V was applied for 30–420 s to deposit the layer. Coated electrodes were air dried and weighed

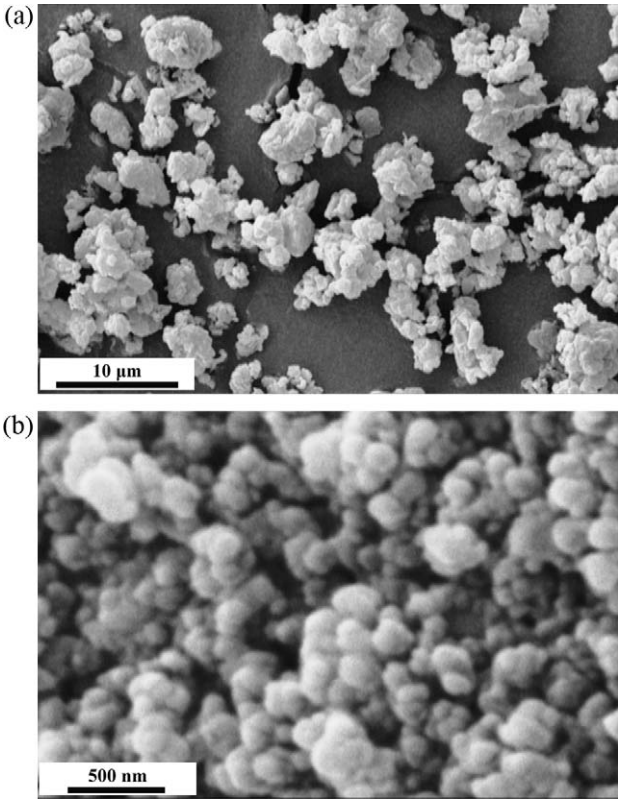

Fig. 1. Morphology of as-received powders: (a) m-AlN and (b) n-AlN particles.

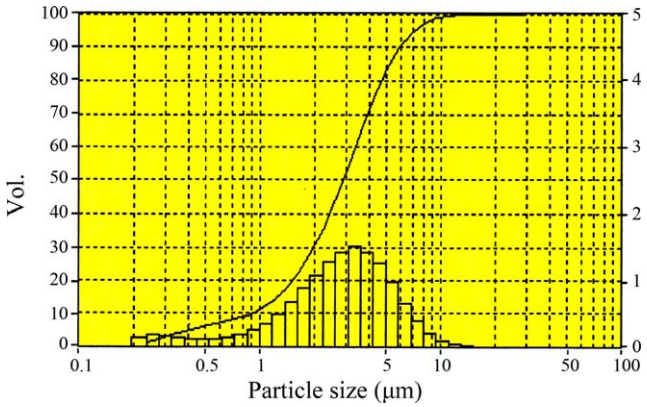

Fig. 2. Particle size distribution of as-received m-AlN.

by a digital balance (Model Sartorius CP324S). Wet samples were also weighed to determine the drying behavior. Microstructural observations were performed by both optical and scanning electron microscope (Cambridge S360).

3. Results and discussion

Parabolic deposition behavior was observed during all experiments. Fig. 3 depicts micro- and nano-suspension weights of the layers formed on the substrate. According to the kinetic equation proposed by Zhang et al. [33] based on the mass conservation law, the weight of the deposit (w) can be expressed as an exponential function of the time of the reaction:

$$w = w_0(1 - e^{-kt}) \quad (3)$$

where w_0 is the initial weight of the powder in the suspension, t is the time and k is the kinetic constant.

As shown in Fig. 3, the experimental and the calculated data indicate good agreement. The correlation coefficient is 0.99 for both nano- and micro-powders. This indicates that Eq. (3) is a suitable enough for explaining the behavior of the deposition rate. Fig. 3 shows that higher yields can be obtained by using micro-powder. Rate constant of the deposition, k, is higher for micro-powder (6.47 s^{-1} for m-AlN) than for nano-powder (4.47 s^{-1} for n-AlN). According to the literature [33], k is expressed as follows:

$$k = \frac{A\varepsilon\zeta}{4\pi V\eta}(E - \Delta E) \quad (4)$$

where A is the surface area of the target electrode, V is the slurry volume, ε is the dielectric constant of the liquid, ζ is the zeta potential of the particle in the solvent, η is the viscosity of the solvent, E is the applied d.c. voltage and ΔE the voltage drop across the deposited layer.

Experimental results showed that zeta potential is the main influencing factor in Eq. (3).

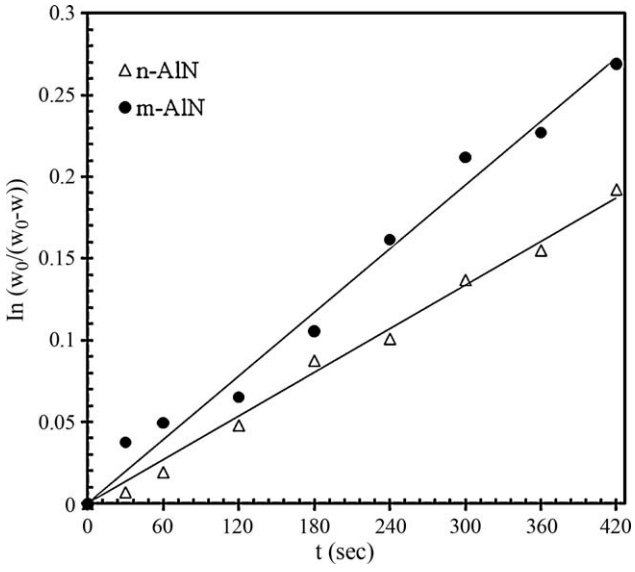

Fig. 3. Relationship between weight (w) and deposition time (t) for m-AlN and n-AlN coatings at 100 V.

Zeta potential is a function of the surface charge of a particle, any adsorbed layer at the interface and the nature and composition of the surrounding medium in which the particle is suspended [34]. The particles were assumed rigid with comparable asperities (according to microscopic observations) and zeta potential was calculated using Smoluchowsky's model [35], which considers particles as hard spheres. As Fig. 4 indicates, the magnitude of the ζ-potential was found to decrease as the particle size decreased. In fact, the small particle size or high surface area contributes to increase electrolyte concentration due to the dissociation of soluble species and ionizable surface sites on the AlN particles [36–38]. In the case of micro-powder, itself, coarse particles moved towards and were deposited on deposition electrode, according to microscopic observations (Fig. 6). The increment of zeta potential with particle size is previously reported by other researchers [34,36–39]. One can thus conclude that because of higher zeta potential (ζ) and therefore kinetic constant (k), the obtained yield (w) will increase with size of the particles.

Parabolic behavior of growth rate is resulted from two main factors: (i) shielding effect of growing layer which causes voltage drop across the deposited layer because of its insulation behavior and (ii) the effective concentration drop originating from migration of particles from suspension to the substrate and their settlement due to the voltage effect. As previously reported by Zhitomirsky and Gal-or [40], during deposition of hydroxyapatite, the applied electric field affects on the

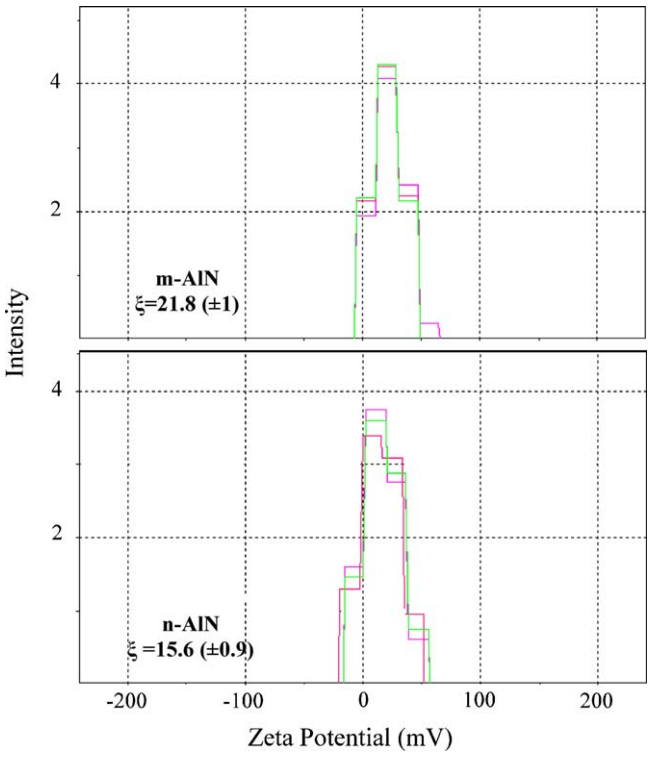

Fig. 4. Zeta potential measurement of suspensions with iodine as an additive. Each sample was measured three times and standard deviations are indicated in brackets.

interactions between particles, leading to subsequent aggregation and sedimentation. These effects are more pronounced for larger particles because of the gravitation effects.

Fig. 5 shows the fracture surface of the EPD deposits produced in this research. As is seen, the corresponding microstructure of the n-AlN resembles more of close-packed appearance than the m-AlN. This is resulted from three major factors: (i) the lower deposition rate, k, of nano-slurry, which offers nanoparticles more time to sit at closest possible packing positions; (ii) the smaller size of the nanoparticles which provide greater option for nanoparticles accommodation; (iii) the greater the surface roughness, shape irregularity, and the aspect ratio of the m-AlN particles, because particles with rough surface textures or shapes suffer from agglomeration due to increased inter-particle friction [41–44]. It must also be taken into account that particles have a range of sizes which may have effects on electrokinetic behavior. Although the difference between particle size of n-AlN and m-AlN is significant (both average and distribution), their centrifugal classification seems useful to assure that particle size distribution and/or the classification procedure do not influence the packing characteristics of the powders. The packing efficiency of solid particles in a wet coating may influence its drying behaviors, such as green density and critical cracking thickness [45].

Both suspension experiments resulted in homogenous tightly packed microstructures. Although a significant difference was not observable, the n-AlN deposit exhibited more packed structure. In other words, deposit from n-AlN was firm and well-shaped indicating that the particles were able to arrange in uniformly dense microstructures (82.07% evaluated by BET).

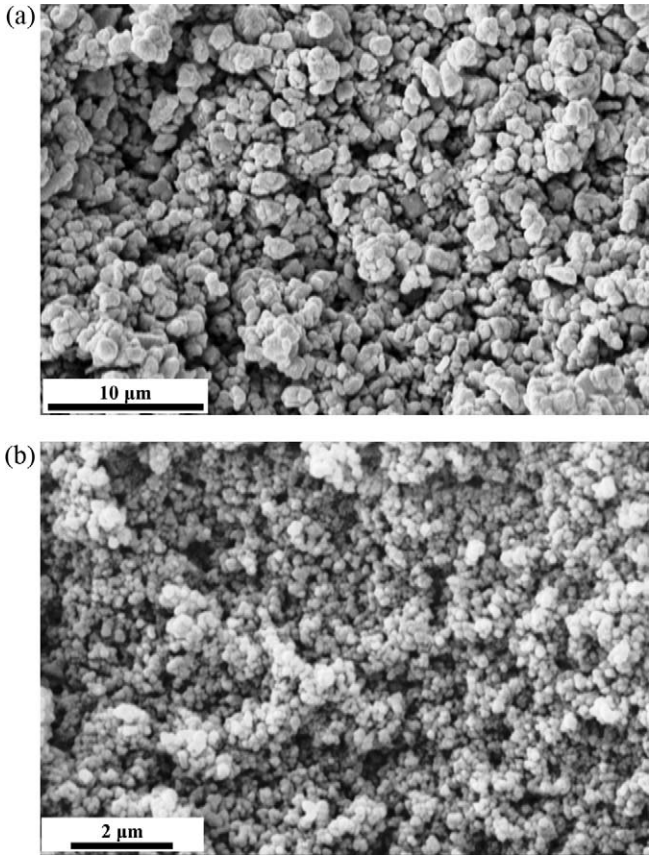

Fig. 5. Fracture surface of green deposits after 240 s EPD and drying: (a) m-AlN and (b) n-AlN.

Fig. 6 shows SEM micrographs of m-AlN and n-AlN coatings obtained by 240 s EPD at 100 V and then drying of the layers. At the top surface (Fig. 6a and b) homogeneity of both coatings was due to the high stability and well dispersion of the suspension. Coagulation, porosity and inter-particle spacing have not been considerable. This indicates enough repulsive forces to enforce the appropriate positioning of the particles at appropriate spaces.

In contrast to the top view, the bottom of the deposited layer shown in Fig. 6c and d appears less homogeneous. Coarser particles (Fig. 6c) and more agglomerated colloids (Fig. 6d) are also visible in the figure. This provides good evidence of higher electrophoretic mobility (or zeta potential) of coarse particles (Fig. 4). A gradual microstructure is thus considered for the deposited film. This means a loose bottom and a dense top which both are in line with previous observations of other investigators [20,24]. On account of the fact that the effective field is maximum in the beginning of the deposition, the required time is so short that the particles cannot arrange in close-packed configuration. A loose packed structure is thus formed near the substrate. As deposition proceeds, the electric field is reduced due to the shielding effect of the resistive layer. Particles achieve, hence, longer times to locate in a more close-packed configuration and a denser microstructure.

The particle packing behavior is almost dictated by kinetic parameters. The most influencing stricture is the applied voltage [41]. A voltage range is, generally, applicable to obtain a uniform and pervasive deposition below which deposition fails to occur because of insufficient driving force for particle migration. Above this range, the uniform electrical flow is disrupted and particles are not given enough time to sit/find the best position with a lateral motion after reaching the as-deposited particles. The resulted microstructure is hence more porous.

Another parameter affecting the film microstructure is the duration of deposition. Fig. 6a shows that when deposition proceeds, pores become finer and more uniformly distributed near the surface of the layer. At the bottom, less uniform size and distribution is, however, obtainable (Fig. 6c). As a consequence, when a thin coating is desired, it would be worth to obtain a fast-formed homogenous layer. It should be also taken into account that although the selected voltage and time resulted in homogenous and uniform coatings from both suspensions (to reveal the particle size effect), further experiments are needed if the optimum conditions are to be explored for deposition (such as optimum physical and chemical parameters).

Fig. 7 compares the optical micrographs of green compacts electrophoretically coated and then dried at ambient atmosphere. The microparticles form a crack-free coating; but nanoparticles break into numerous fragments. The origin of the drying stress which causes the crack occurrence is bulk shrinkage [46] due to the coating contraction in the thickness

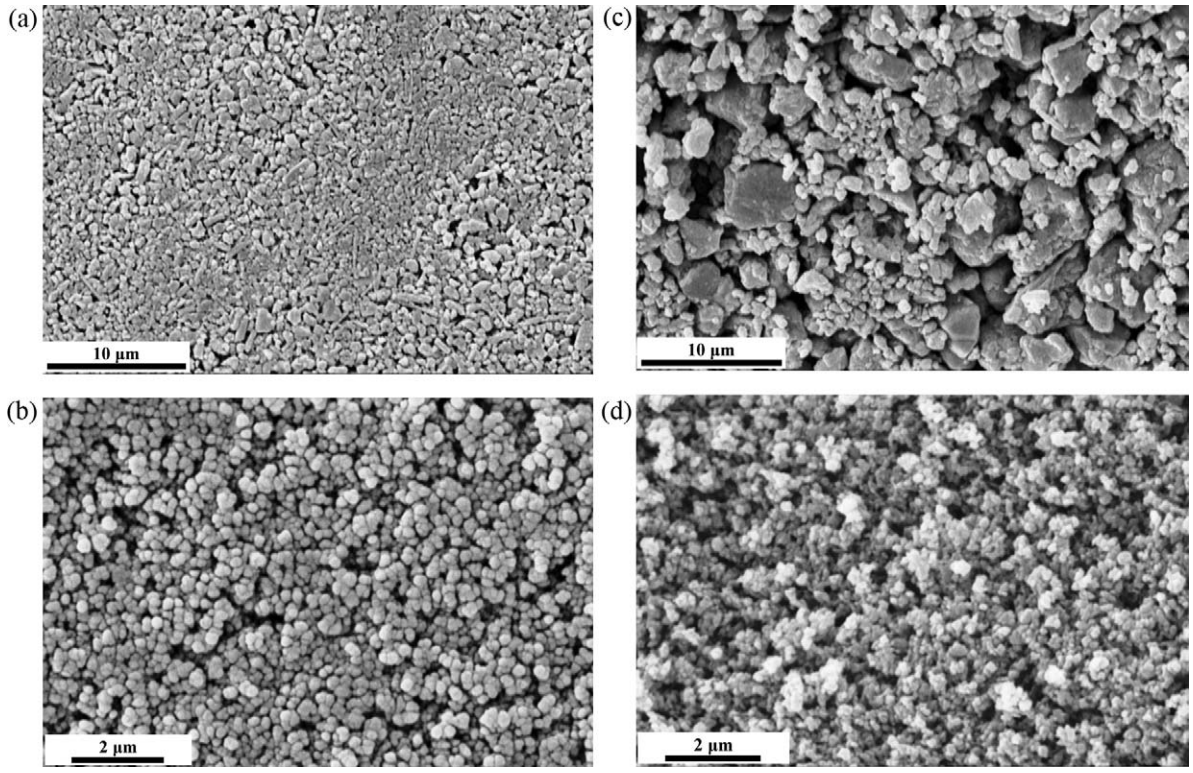

Fig. 6. Micrographs of coatings from top surface: (a) m-AlN, (b) n-AlN and bottom: (c) m-AlN and (d) n-AlN after 240 s EPD and drying, the pore structure becoming more uniform and smaller in size as well as distribution from bottom to top.

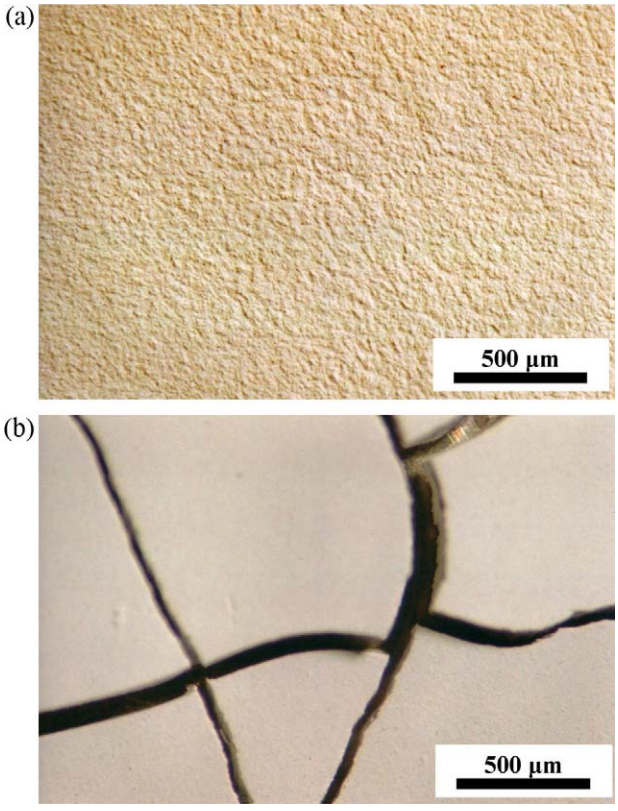

Fig. 7. Optical micrograph of the surface of coatings after 240 s EPD and drying: (a) m-AlN and (b) n-AlN.

direction caused by the water evaporation. Since the in-plane shrinkage is constrained by the substrate, the biaxial tensile stress arises and leads to crack formation. It is proved that the in-plane stress is the result of capillary pressure [47]:

$$P = -\frac{2\gamma_{lv}}{r_p} \tag{5}$$

where γ_{lv} is the surface tension of the solvent and r_p is the characteristic pore dimension. Lower capillary forces produced by the microparticles (due to larger mean pore size) result in smaller tensile stresses which are not large enough to crack the coatings. Crack-free coatings are hence produced by EPD of slurry having microparticles. Contrary to this effect, in EPD of nanoslurry mixture, because the capillary length is shorter than the specimen half-length, liquid is drained from the edge of the air–solvent interface producing pores and cracks [48].

In order to obtain a flaw-free coating with uniform surface and homogenous microstructure, drying must be considered as important as deposition conditions. Fig. 8 shows the sample weight as a function of the drying duration. The slope of the curve is a useful tool for making a good correlation between the slurry characteristics, the drying behavior and the final green microstructure [49].

Both curves may roughly be divided into two segments: (i) an initial linear segment called constant-rate period (CRP) and (ii) a subsequent falling-rate period (FRP). In the CRP, evaporation occurs at the exterior of the layer supplying the

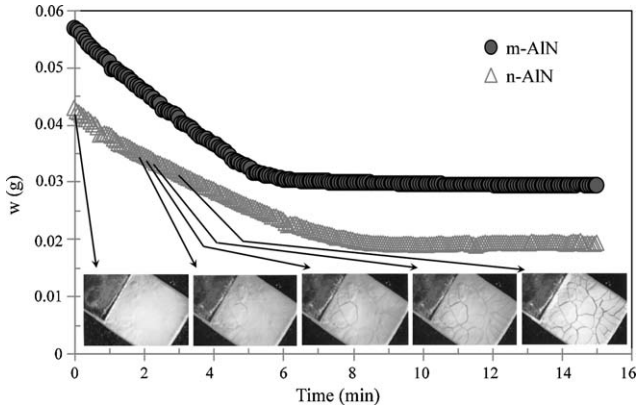

Fig. 8. Weight versus time of coating prepared from m- and n-AlN, and sequence of optical images taken as a function of drying time from nano-slurry.

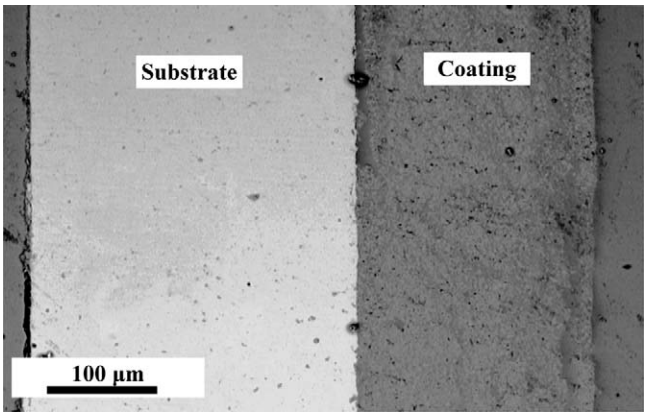

Fig. 9. Interface of substrate/coatings from m-AlN after 240 s EPD.

fluid via capillary-driven transport to the surface of the exterior [47]. The transition to the FRP happens when fluid can no longer be supplied to the exterior with the initial rate. Owing to the increased distance of the drying front from the coating surface, the slope begins to decrease. Capillary forces are still, however, operative to transport the solvent to the exterior (first step of FRP). With further evaporation, solvent resides in isolated pores and removed from interior only by vapor-phase diffusion (second step of FRP). Distinction between these stages is difficult especially for nanoslurry mixture because of forming the cracks which expose new evaporation sites and activate more capillaries within the sample. As a result, decrease trend of the corresponding curve is reduced within a broader time range. Earlier transition from CRP to FRP for nanoslurry mixture is also related to shortness of capillaries which are no longer able to transport the solvent to the layer exterior. The dominant mechanism changes hence and the vapor-phase diffusion substitute the capillary action.

A comprehensive discussion has been given by Lan et al. [48,50–52]. They have related the slope of the drying curve to such variables as specific surfaces [51]. Steeper slope of the micromixture as compared to that of the nanoslurry in the CRP stage can thus be attributed to the larger pore size and lower specific area of the former.

The inset of Fig. 8 shows the sequence of optical images taken as a function of the drying duration from nanoslurry at 0, 120, 130, 140 and 180 s. Drying of the coating is observed to start from the edge. This is termed ‘lateral drying’ [48,50]. Due to the higher evaporation rates, particles first densely pack at the coating edge. High capillary forces develop at the exterior as compared to the interior where slurry is well fluidized to release any constrained stress due to the viscous flow. A pressure gradient in the horizontal direction forms hence along the coating surfaces and drives solvent and free particles from the center towards the edges [50]. Transition from CRP to FRP results in reduction of the solvent in the upper layer causing formation of a stress gradient in the vertical direction across the thickness. Higher compressive stress is therefore obtained in the upper layers causing the particle network to contract [46]. The fragments gradually fold up hence and detach from the substrate relaxing the stress. Although nanoslurry is of high potential to contain cracks after drying, the degree of cracks is expected to decrease considerably after the sintering process [53].

In contrast to the above discussion, no evidence is observed of delamination and/or segregation at the interface of m-AlN coating with substrate (Fig. 9). This indicates that the network is solid enough to tolerate imposed stresses which result from the constrained volume shrinkage and the tolerable capillary forces. The typical thickness of the coating was evaluated to be about 230 μm.

4. Conclusions

Electrophoretic coatings were fabricated from micro- and nano-sized aluminum nitride powders suspended in non-aqueous slurry mixtures. The process was conducted under constant voltage because its feasibility and different time durations. Kinetics of EPD process obeyed a parabolic equation correlating the coating yield to the deposition duration. Due to the higher zeta potential, coarser microparticles and agglomerated nanoparticles were deposited from their suspensions at the beginning. The layer became more uniform and dense with the deposition duration. A smooth surface was obtained after 420 s from both suspensions. Crack-free surfaces were obtained by ambient drying of the microslurry EPD layers; while nanocoatings produced under these conditions were fragmented and delaminated from the substrate. Due to the difference in the capillary scale, micro-coating showed higher drying rate than nano-coating and no evidence of segregation and debonding appeared in the former. In deposition from nanoslurry suspension, tensile stress induced from small capillary size and stress gradient across thickness due to the lateral drying caused, however, fragmentation and delamination.

References

[1] X.Y. Guo, J. Gough, P. Xiao, Electrophoretic deposition of hydroxyapatite coating on Fecralloy and analysis of human osteoblastic cellular response, J. Biomed. Mater. Res. A 80 (2007) 24–33.
[2] D. Stojanovic, B. Jokic, D. Veljovic, R. Petrovic, P.S. Uskokovic, D. Janackovic, Bioactive glass-apatite composite coating for titanium

implant synthesized by electrophoretic deposition, J. Eur. Ceram. Soc. 27 (2007) 1595–1599.
[3] N. Nagarajan, P.S. Nicholson, Nickel–alumina functionally graded materials by electrophoretic deposition, J. Am. Ceram. Soc. 87 (2004) 2053–2057.
[4] M. Popa, P. Hvizdos, G. Anne, J.M. Calderon-Moreno, Thermal residual stress gradients in an alumina–zirconia composite obtained by electrophoretic deposition, J. Am. Eur. Soc. 26 (2006) 553–558.
[5] Y.J. Wu, J. Li, H. Tanaka, M. Kuwabara, Preparation of nano-structured $BaTiO_3$ thin film by electrophoretic deposition and its characterization, J. Am. Ceram. Soc. 25 (2005) 2041–2044.
[6] J. Zhang, B.I. Lee, Electrophoretic deposition and characterisation of micrometer-scale $BaTiO_3$ based X7R dielectric thick films, J. Am. Ceram. Soc. 83 (2000) 2417–2422.
[7] J. Ma, C. Wang, K.W. Peng, Electrophoretic deposition of porous hydroxyapatite scaffold, Biomaterials 24 (2003) 3505–3510.
[8] A.R. Boccaccini, J.A. Roether, B.J.C. Thomas, M.S.P. Shaffer, E. Chavez, E. Stoll, E.J. Minay, The electrophoretic deposition of inorganic nanoscaled materials, J. Ceram. Soc. Jpn. 114 (2006) 1–14.
[9] B. Ferrari, R. Moreno, Electrophoretic deposition of aqueous alumina slip, J. Am. Eur. Soc. 17 (1997) 549–556.
[10] R.W. Powers, The electrophoretic forming of beta-alumina ceramic, J. Electrochem. Soc. 122 (1975) 482–486.
[11] X.J. Lu, P. Xiao, Constrained sintering of YSZ/Al_2O_3 composite coatings on metal substrates produced from eletrophoretic deposition, J. Am. Eur. Soc. 27 (2007) 2613–2621.
[12] Z. Peng, M. Liu, Preparation of dense platinum-yttria stabilized zirconia and yttria stabilized zirconia films on porous $La_{0.9}Sr_{0.1}MnO_3$ (LSM) substrates, J. Am. Ceram. Soc. 84 (2001) 283–288.
[13] M. Yousefpour, A. Afshar, J. Chen, X. Zhang, Electrophoretic deposition of porous hydroxyapatite coatings using polytetrafluoroethylene particles as templates, Mater. Sci. Eng. C 27 (2007) 1482–1486.
[14] A.R. Boccaccini, J. Cho, J.A. Roether, B.J.C. Thomas, E.J. Minay, M.S.P. Shaffer, Electrophoretic deposition of carbon nanotubes, Carbon 44 (2006) 3149–3160.
[15] A.R. Boccaccini, I. Zhitomirsky, Application of electrophoretic and electrolytic deposition techniques in ceramics processing, Curr. Opin. Solid State Mater. Sci. 6 (2002) 251–260.
[16] M. Zarbov, D. Brandon, N. Cohen, L. Shemesh, Engineering performance in applied EPD: problems and solutions, J. Mater. Sci. 41 (2006) 8115–8122.
[17] O.O.V.d. Biest, L.J. Vandeperre, Electrophoretic deposition of materials, Annu. Rev. Mater. Sci. 29 (1999) 327–352.
[18] Y. Fukada, N. Nagarajan, W. Mekky, Y. Bao, H.S. Kim, P.S. Nicholson, Electrophoretic deposition—mechanisms, myths and materials, J. Mater. Sci. 39 (2004) 787–801.
[19] P. Sarkar, P.S. Nicholson, Electrophoretic deposition (EPD): mechanisms, kinetics, and application to ceramics, J. Am. Ceram. Soc. (1996) 1987–2002.
[20] C.Y. Chen, S.Y. Chen, D.M. Liu, Electrophoretic deposition forming of porous alumina membranes, Acta Mater. 47 (1999) 2717–2726.
[21] Y.C. Wang, I.C. Leu, M.H. Hon, Kinetics of electrophoretic deposition for nanocrystalline zinc oxide coatings, J. Am. Ceram. Soc. 87 (2004) 84–88.
[22] K. Kishigawa, Y. Hirata, Packing density and consolidation energy of flocculated aqueous SiC suspension, J. Am. Eur. Soc. 26 (2006) 217–221.
[23] R.C. Chiu, M.J. Cima, Drying of granular ceramic films: II, drying stress and saturation uniformity, J. Am. Ceram. Soc. 76 (1993) 2769–2777.
[24] C.Z. Ji, I.P. Shapiro, P. Xiao, Fabrication of yttria-stabilized-zirconia coatings using electrophoretic deposition: effects of agglomerate size distribution on particle packing, J. Am. Eur. Soc. 29 (2009) 3167–3175.
[25] J.A. Lewis, Colloidal processing of ceramics, J. Am. Ceram. Soc. 83 (2000) 2341–2359.
[26] P. Sarkar, D. De, H. Rho, Synthesis and microstructural manipulation of ceramics by electrophoretic deposition, J. Mater. Sci. 39 (2004) 819–823.
[27] R.S. Hyam, K.M. Subhedar, S.H. Pawar, Effect of particle size distribution and zeta potential on the electrophoretic deposition of boron films, Colloids Surf. A: Physicochem. Eng. Aspects 315 (2008) 61–65.
[28] K. Königa, S. Novaka, A.R. Boccaccini, S. Kobea, The effect of the particle size and the morphology of alumina powders on the processing of green bodies by electrophoretic deposition, J. Mater. Process. Technol. 210 (2010) 96–103.
[29] R.S. Hyam, K.M. Subhedar, S.H. Pawar, Suspension stability studies for the electrophoretic deposition of boron films, Colloids Surf. A: Physicochem. Eng. Aspects 297 (2007) 172–178.
[30] S.A. Guelcher, Y. Solomentsev, J.L. Anderson, Aggregation of pairs of particles on electrodes during electrophoretic deposition, Powder Technol. 110 (2000) 90–97.
[31] S.T. Aruna, K.S. Rajam, A study on the electrophoretic deposition of 8YSZ coating using mixture of acetone and ethanol solvents, Mater. Chem. Phys. 11 (2008) 131–136.
[32] K. Nobuyuki, T. Takeyo, S. Hiromasa, H. Touru, Preparation of various oxide films by an electrophoretic deposition method: a study of the mechanism, Jpn. J. Appl. Phys. Part 1: Regular Papers & Short Notes & Review Papers 34 (1995) 1643–1647.
[33] Z. Zhang, Y. Huang, Z. Jiang, Electrophoretic deposition forming of SiC-TZP composites in a nonaqueous sol media, J. Am. Ceram. Soc. 77 (1994) 1946–1949.
[34] H.-K. Lee, H.-Y. Lee, J.-M. Jeon, Codeposition of micro- and nano-sized SiC particles in the nickel matrix composite coatings obtained by electroplating, Surf. Coat. Technol. 201 (2007) 4711–4717.
[35] M.v. Smoluchowski, In: Handbuch der Electrizität und des Magnetismus (Graetz), vol. II, Barth, Leipzig, 1921, p. 366.
[36] H.B. Bull, R.A. Gortner, Electrokinetic potentials. X. The effect of particle size on the potential, J. Phys. Chem. 36 (1932) 111–119.
[37] S. Jailani, G.V. Franks, T.W. Healy, ζ potential of nanoparticle suspensions: effect of electrolyte concentration, particle size, and volume fraction, J. Am. Ceram. Soc. 91 (2008) 1141–1147.
[38] C. Tallon, M. Limacher, G.V. Franks, Effect of particle size on the shaping of ceramics by slip casting, J. Am. Eur. Soc. 30 (2010) 2819–2826.
[39] A. Kitahara, T. Fujii, S. Katano, Dependence of ζ-potential upon particle size and capillary radius at streaming potential study in nonaqueous media, Bull. Chem. Soc. Jpn. 44 (1971) 3242–3245.
[40] I. Zhitomirsky, L. Gal-or, Electrophoretic deposition of hydroxyapatite, J. Mater. Sci. 8 (1997) 213–219.
[41] R.K. McGeary, Mechanical packing of spherical particles, J. Am. Ceram. Soc. 44 (1961) 513–522.
[42] G.L. Messing, G.Y. Onada, Inhomogeneity-packing density relations in binary powders, J. Am. Ceram. Soc. 61 (1978) 1–5.
[43] M.N. Rahaman, Ceramic processing and sintering, Marcel Dekker, New York, 2003.
[44] M.D. Sacks, J.A. Pask, Sintering of mullite-containing materials:II. Effect of agglomeration, J. Am. Ceram. Soc. 65 (1982) 71–77.
[45] C. Ji, W. Lan, P. Xiao, Fabrication of yttria-stabilized zirconia coatings using electrophoretic deposition: packing mechanism during deposition, J. Am. Ceram. Soc. 91 (2008) 1102–1109.
[46] J.A. Lewis, K.A. Blackman, A.L. Ogden, J.A. Payne, L.F. Francis, Rheological property and stress development during drying of tape-cast ceramic layers, J. Am. Ceram. Soc. 99 (1996) 3225–3234.
[47] G.W. Scherer, Theory of drying, J. Am. Ceram. Soc. 73 (1990) 3–14.
[48] W. Lan, P. Xiao, Drying stress of yttria-stabilized-zirconia slurry on a metal substrate, J. Am. Eur. Soc. 27 (2007) 3117–3125.
[49] G. Tarì, J.M.F. Ferreira, O. Lyckfeldt, Influence of the stabilising mechanism and solid loading on slip casting of alumina, J. Am. Eur. Soc. 18 (1998) 479–486.
[50] W. Lan, X. Wang, P. Xiao, Agglomeration on drying of yttria-stabilised-zirconia slurry on a metal substrate, J. Am. Eur. Soc. 26 (2006) 3599–3606.
[51] W. Lan, P. Xiao, Constrained drying of aqueous yttria-stabilized zirconia slurry on a substrate. I: Drying mechanism, J. Am. Ceram. Soc. 89 (2006) 1518–1522.
[52] W. Lan, P. Xiao, Constrained drying of an aqueous yttria-stabilized zirconia slurry on a substrate II: binary particle slurry, J. Am. Ceram. Soc. 90 (2007) 2771–2778.
[53] T. Moskalewicz, A. Czyrska-Filemonowicz, A.R. Boccaccini, Microstructure of nanocrystalline TiO_2 films produced by electrophoretic deposition on Ti–6Al–7Nb alloy, Surf. Coat. Technol. 201 (2007) 7467–7471.